Sowshank Attention

Every pixel deserves a second chance

National Technical University of Athens
School of Electrical and Computer Engineering

Evangelos Chaniadakis
echaniadakis@gmail.com
03400279

Submission Date
May 16, 2025

Contents

Chapter I

Introduction

This work tackles the challenge of classifying crop types using satellite-based time series data. Specifically, we focus on the *TimeMatch* dataset, which contains multispectral time series data collected from Sentinel-2 imagery. The dataset covers agricultural parcels across four distinct regions in Europe, providing valuable insights into crop classification. While the broader aim of TimeMatch is to support various agricultural tasks like crop classification and domain adaptation across different regions, this study zooms in on crop classification for a specific region and timeline. For practical purposes, we utilize a substantially reduced subset of the dataset, provided by the course instructor via Google Drive, which specifically corresponds to the Denmark region for the year 2017. The goal is to develop a reliable pipeline for classifying agricultural parcels into one of 15 crop types. The model is designed to effectively classify crop types by leveraging the spatiotemporal nature of satellite time series data. It begins with a Pixel Set Encoder, which captures spatial relationships within each parcel by processing pixels, outputting only temporal and feature dimensions. A Transformer Encoder is then used to capture temporal dynamics, enhanced by sinusoidal temporal positional encodings derived from the acquisition dates of the samples. A classification token aggregates the temporal information, allowing the model to focus on the overall trends. Subsequently, a custom Multi-Layer Perceptron is employed to perform the final classification, enabling accurate identification of crop types across the dataset.

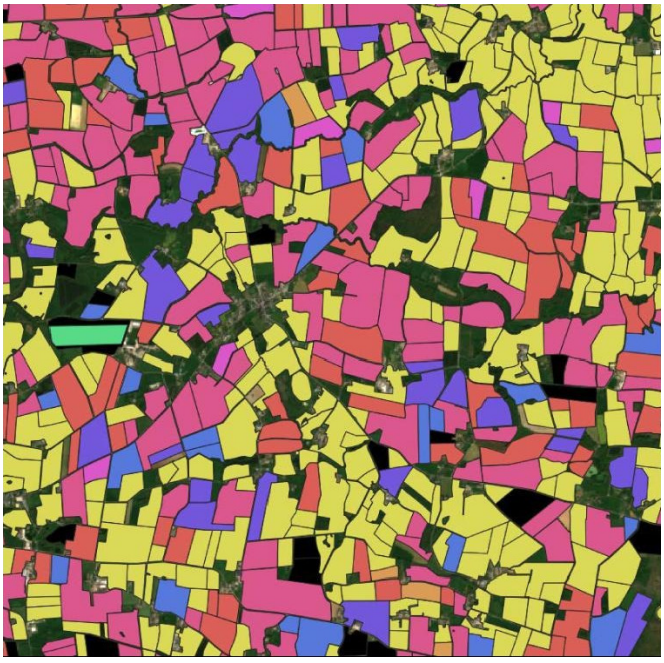

Figure I: Ground truth crop type labels in a sample region of the *TimeMatch* dataset.

Chapter II

Dataset

The TimeMatch dataset is a satellite-derived, multivariate time series dataset developed to support research in remote sensing and temporal modeling. It is based on Sentinel-2 imagery and captures the seasonal dynamics of agricultural parcels across multiple regions in Europe. The dataset is designed to facilitate a deeper understanding of vegetation phenology by providing rich spectral and temporal information at the pixel level.

I Geographical & Chronological Coverage

TimeMatch comprises data from four geographically and climatologically distinct European countries: France, Spain, Italy and Denmark. Each region includes agricultural parcels observed over a single year. Imagery is uniformly sampled on a weekly basis, resulting in 52 temporally aligned acquisitions per year. All data is derived from Sentinel-2 Level-2A products, ensuring consistent surface reflectance calibration.

II Spectral & Temporal Characteristics

Each pixel's time series consists of 52 weekly observations across 10 selected spectral bands:

- Blue (B2), Green (B3), Red (B4)
- Red Edge (B5, B6, B7)
- Near-Infrared (B8, B8A)
- Short-Wave Infrared (B11, B12)

These bands, selected for their sensitivity to vegetation traits like chlorophyll, biomass and water stress, produce a 52×10 matrix per pixel, with temporal alignment across all pixels in a parcel.

$$\text{Pixel Data} \in R^{52 \times 10}$$

III Hierarchical Structure

The dataset is structured hierarchically:

$$\text{Region} \rightarrow \text{UTM Tile} \rightarrow \text{Year} \rightarrow \text{Parcel} \rightarrow \text{Pixel} \rightarrow \text{Time Series}$$

At the top level, data are grouped by region and subdivided into Universal Transverse Mercator (UTM) tiles. Each tile contains data for a specific year, further organized into parcels, each representing an agricultural field. Parcels are composed of multiple pixels at 10-meter resolution, in accordance with Sentinel-2 standards. Each pixel is represented by a time series of length 52, with 10 spectral bands per time step.

The dataset is organized under the root directory with the following structure:

```
timematch_data
    denmark
        32VNH
            2017
                data
                    0.zarr
                        .zarray
                        0.0.0
                        0.1.0
                        1.0.0
                        1.1.0
                    1.zarr
                        .zarray
                        0.0.0
                        1.0.0
                    2.zarr
                    3.zarr
                    4.zarr
                meta
                    blocks
                        blocks_denmark_32VNH_2017.shp
                        blocks_denmark_32VNH_2017.shx
                        blocks_denmark_32VNH_2017.dbf
                        blocks_denmark_32VNH_2017.prj
                        blocks_denmark_32VNH_2017.cpg
                    dates.json
                    labels.json
                    filtered_labels.json
                    normalization_stats.json
                    metadata.pkl
```

Data Files (data/)

Each file in the data/ directory (e.g., 0.zarr, 1.zarr) contains a single parcel stored in Zarr format. Each parcel directory includes:

- .zarray: Metadata about array shape, chunking and data type.
- Binary chunks named using Zarr's internal indexing scheme (e.g., 0.0.0, 1.0.0, 0.1.0).

Each Zarr array stores a 3D tensor of shape $(52, 10, n_p)$ representing:

- 52 weekly time steps,
- 10 spectral bands,
- n_p pixels (variable per parcel).

Metadata Files (meta/)

The meta/ directory contains essential auxiliary files for dataset interpretation and spatial referencing:

- dates.json — JSON file listing the 52 acquisition dates common to all parcels in the year-tile, enabling temporal alignment of the time series data.
- labels.json — JSON mapping parcel IDs to their crop class labels, providing categorical annotations for supervised tasks.
- filtered_labels.json — JSON file with filtered crop labels after preprocessing.
- metadata.pkl — A pickled Python dictionary containing parcel-level metadata such as:
  - id (string) — parcel identifier,
  - label (float) — numeric crop class,
  - n_pixels (integer) — number of pixels in the parcel,

  - block (integer) — identifier linking the parcel to a spatial block,
  - geometric_features (list of floats) — shape descriptors or spatial metrics (e.g., area, perimeter, compactness).
- blocks/ directory — contains shapefile components that together define the exact spatial boundaries of parcels:
  - .shp — main file storing parcel polygon geometries,
  - .shx — index file linking geometry records for efficient access,
  - .dbf — attribute table storing tabular parcel information (IDs, labels, etc.),
  - .prj — coordinate reference system (CRS) definition, specifying spatial projection (e.g., UTM),
  - .cpg — text encoding of the attribute table, ensuring correct character representation.

The directory also includes two files generated during preprocessing, detailed later.

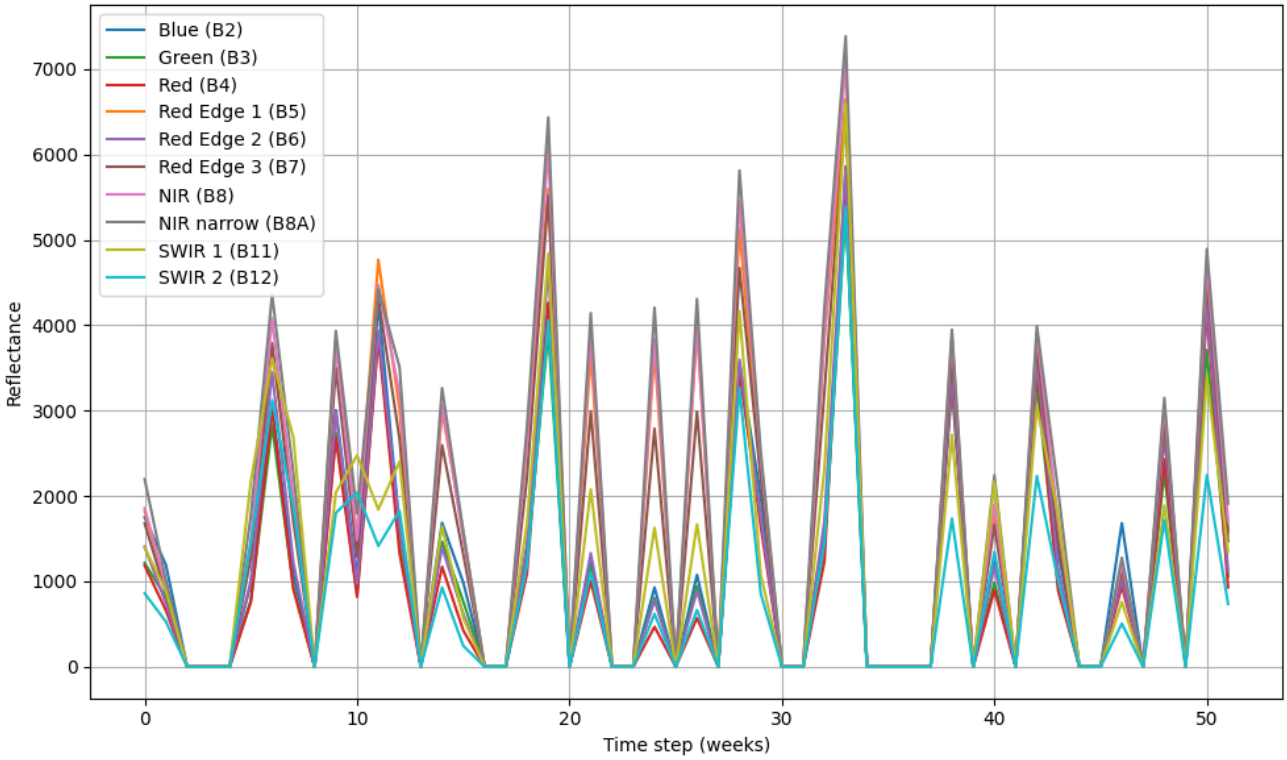

The figure above illustrates the spectral time series for a single pixel 0 from parcel 0 of the Denmark 2017 subset, showcasing reflectance across all 10 bands. Reflectance values range from 0 to 7000, measured weekly over the 52-week period, corresponding to a full agricultural cycle. The reflectance profiles exhibit distinct seasonal variations, with pronounced peaks between weeks 17–20 (late April to mid-May) and weeks 31–35 (early August to early September). These periods likely correspond to critical phenological stages in Danish agricultural cycles: the spring peak aligning with rapid vegetative growth and the late-summer peak reflecting senescence and harvest activities. Such temporal patterns are characteristic of temperate cropping systems and underline the importance of capturing seasonal dynamics for accurate classification. The NIR (B8) and Narrow NIR (B8A) bands display the highest reflectance, exceeding 6000 at their peaks, due to their sensitivity to vegetation biomass and canopy structure. The Red Edge bands (B5–B7) show intermediate reflectance, peaking around 4000–6000, reflecting their utility in detecting transitions in vegetation health. In contrast, the Blue (B2) and Red (B4) bands exhibit lower reflectance, due to chlorophyll absorption during active growth phases. The SWIR bands (B11, B12) demonstrate more stable reflectance, typically below 4000, indicative of their sensitivity to soil moisture and water content, which varies less dramatically over the season.

Chapter III

Pre-processing

The preprocessing stage is a critical component of the crop classification pipeline, ensuring that the *TimeMatch* dataset is appropriately cleaned, filtered and normalized for downstream model training. This chapter details the two primary preprocessing steps: category filtering and indexing and data normalization. These steps address class imbalance, remove noisy or underrepresented data and standardize the spectral reflectance values to facilitate robust model performance. The implementation is provided in two scripts: category_preprocessing.py and normalization.py, which operate on the Denmark 2017 subset of the dataset.

I Category Filtering and Indexing

The first preprocessing step involves filtering and reindexing the crop type labels to ensure a balanced and representative dataset. The raw labels are stored in labels.json within the meta/ directory, mapping parcel IDs to their corresponding crop type labels. Due to the presence of underrepresented classes, which could negatively impact model training, we filter out categories with insufficient samples and assign new indices to the remaining classes.

We load the label data from labels.json and calculate the frequency of each crop type. For the Denmark 2017 dataset, the initial category counts are

Class	Count
corn	275
spring_barley	1140
meadow	1013
winter_wheat	856
winter_rapeseed	301
unknown	511
winter_barley	352
winter_rye	316
spring_peas	17
spring_oat	120
horsebeans	28
winter_triticale	42
spring_wheat	26
spring_triticale	2

Table I: Category Counts

To ensure robust model training, we exclude crop types with fewer than a minimum number of samples, defined as 200. For the Denmark 2017 dataset, this results in 8 retained classes, as several categories (e.g., spring_peas, spring_oat, spring_triticale) have fewer than 200 samples.

After filtering, the remaining 8 labels are reindexed to create a contiguous set of class indices suitable for model training. We assign indices to labels, prioritizing the unknown class to ensure it receives index 0, while sorting other labels in descending order of their respective counts, ensuring that more frequent classes receive lower indices. For the Denmark 2017 dataset, the filtered label indexing is:

Class	**Index**
unknown	0
spring_barley	1
meadow	2
winter_wheat	3
winter_barley	4
winter_rye	5
winter_rapeseed	6
corn	7

Table II: Filtered Label Indexing

The finalized dataset comprises 4,764 land parcels categorized into eight distinct classes. The corresponding labels are stored in the filtered_labels.json file within the metadata directory. To facilitate a better understanding of these crop categories, we provide representative images below, offering the reader a clear visual insight into their typical appearance and distinguishing features.

(a) Spring Barley

(b) Meadow

(c) Winter Wheat

(d) Winter Barley

(e) Winter Rye

(f) Winter Rapeseed

(g) Corn

Figure I: Representative visual examples of each the resulting land cover classes.

II Feature Extraction

To enrich the spectral representation of crop parcels, we compute two widely adopted vegetation indices: the Normalized Difference Vegetation Index (NDVI) and the Enhanced Vegetation Index (EVI). These indices, as introduced by Huete et al. (2002), are commonly used in remote sensing for assessing plant health, growth stages, and overall vegetation dynamics. By incorporating these biologically meaningful features, we aim to improve the model's discriminative power for crop classification.

NDVI quantifies vegetation greenness by exploiting the strong reflectance of healthy vegetation in the near-infrared (NIR) spectrum and its absorption in the red spectrum. It is defined as the normalized difference between NIR and red reflectance, thereby enhancing the contrast between vegetated and non-vegetated surfaces.

EVI extends NDVI by integrating the blue band, which helps correct for atmospheric disturbances and soil background effects. This makes EVI particularly advantageous in conditions with high vegetation density and varying atmospheric interference—conditions frequently observed in our dataset, which exhibits an average cloud cover of 40.86%.

The NDVI and EVI values are computed per pixel and per time step using the following formulations:

$$\text{NDVI} = \frac{\text{NIR} - \text{Red}}{\text{NIR} + \text{Red} + 10^{-10}}$$

$$\text{EVI} = 2.5 \cdot \frac{\text{NIR} - \text{Red}}{\text{NIR} + 6 \cdot \text{Red} - 7.5 \cdot \text{Blue} + 1 + 10^{-10}}$$

where NIR corresponds to band 8 (B8), Red to band 4 (B4), and Blue to band 2 (B2). These indices are appended as additional channels to the existing 10-band input, expanding the feature tensor from $(n_p, T_v, 10)$ to $(n_p, T_v, 12)$, where n_p is the number of pixels per parcel and T_v is the number of time steps.

III Data Augmentation

To enhance the model's generalization and robustness, especially given the limited size of our dataset, we implement data augmentation techniques during training within the $\mathrm{ParcelDataset}$ class. These techniques introduce controlled variability to the spectral and temporal data, simulating real-world conditions such as sensor noise, temporal shifts and atmospheric effects. The augmentation is applied probabilistically to a tensor of shape (N, T, C), where N is the number of sampled pixels (32), T is the number of time steps (52), and C is the number of channels (12). The following techniques are employed:

- **Spectral Jitter**: With a 80% probability, Gaussian noise with a mean of 0 and a standard deviation of 0.05 is added to each channel value, simulating sensor noise or slight variations in reflectance.
- **Time Shift**: With a 50% probability, a random temporal shift between -5 and 5 time steps is applied using a circular shift ($\mathrm{np.roll}$), mimicking slight misalignments in acquisition timing or phenological variations across parcels.
- **Random Band Dropout**: With a 30% probability, 1 to 2 channels are randomly selected and set to zero, simulating missing or corrupted spectral bands due to cloud cover or sensor failure. The number of dropped channels is a randomly selected integer between 1 and 2.

- **Gaussian Blur in Time**: With a 30% probability, a Gaussian filter with a standard deviation of 1.0 is applied along the time axis for each pixel, smoothing the temporal sequence to simulate atmospheric scattering or averaging effects.

IV Data Normalization

The second preprocessing step normalizes the spectral reflectance values across the 10 spectral bands and the extracted features to standardize the data distribution. This is essential for improving model convergence and ensuring that features are on a comparable scale. The normalization statistics are computed over all pixels in the filtered parcels and saved in $\mathrm{normalization\_stats.json}$.

Computing Channel-wise Statistics

The $\mathrm{normalization.py}$ script processes the parcel data stored in Zarr format within the $\mathrm{data/}$ directory. For each of the 4764 parcels listed in $\mathrm{filtered\_labels.json}$, the script loads the corresponding Zarr array (e.g., $\mathrm{0.zarr}$), which originally has shape $(52, 10, n_p)$, representing 52 time steps, 10 spectral bands, and n_p pixels. After augmenting the data with NDVI and EVI, the shape becomes $(52, 12, n_p)$. The data is then reshaped to $(n_p, 52, 12)$ to facilitate pixel-wise computations and then flattened to $(n_p \cdot 52, 12)$ for statistical aggregation. We compute the mean and variance for each spectral band using Welford's online algorithm, which is numerically stable for large datasets. For each pixel's spectral vector $x \in R^{12}$, the running mean and variance are updated as follows:

$$\delta = x - \mu_t$$

$$\mu_{t+1} = \mu_t + \frac{\delta}{t+1}$$

$$M2_{t+1} = M2_t + \delta \cdot (x - \mu_{t+1})$$

where μ_t is the running mean at step t, $M2_t$ is the running sum of squared differences and t is the number of observations processed.

The final mean and standard deviation for each channel are

$$\mu = \mu_T \quad \& \quad \sigma = \sqrt{\frac{M2_T}{T-1}}$$

where T is the total number of pixel observations. This process is applied across all valid parcels, skipping any with missing files or incompatible shapes.

V Cloud Coverage Mitigation

To address the adverse impact of cloud cover, which averages 40.86% across our dataset, we explored a temporal filtering strategy. Specifically, we experimented with selecting the top-K time steps exhibiting the lowest cloud coverage, as measured by the $\mathrm{cloudy\_pct}$ metric. Setting $\mathrm{top\_k} = 32$, we retained the 32 least cloudy observations out of 52 total time steps per parcel. However, this approach did not yield any notable performance improvements. A likely explanation is that the presence of cloud-contaminated observations introduces variability that may act as a form of implicit data augmentation. Consequently, we opted to retain all available time steps, regardless of their cloud coverage levels.

VI Pixel Sampling

Since parcels vary in pixel count, we standardized the input by sampling a fixed number of pixels per parcel ($\mathrm{sample\_pixels} = 32$). Several pixel sampling strategies were investigated to balance representativeness, computational efficiency and predictive performance:

- **K-means clustering**: As introduced by MacQueen (1967), K-means clustering was used to group pixels into three clusters based on their mean spectral signatures. We sampled proportionally from each cluster to promote diversity. However, the method's computational cost ($O(n \cdot k \cdot i)$) and lack of measurable performance improvement led us to discard it.
- **Stratified random sampling**: Following the principles in Thompson (2012), we divided pixels into quartiles based on spectral variance and drew samples evenly from each stratum. Despite its statistical soundness, it did not yield superior results compared to simpler approaches.
- **Farthest Point Sampling (FPS)**: Inspired by the strategy in Eldar et al. (1997), FPS was employed to iteratively select the most spectrally dissimilar pixels. While it ensured diversity in spectral space, its computational overhead and inconsistent performance gains limited its utility.
- **Spatially-aware sampling**: In line with the spatial sampling guidelines discussed by J. Li and Heap (2015), we experimented with methods based on inter-pixel distance or spatial grids. However, due to limited or unreliable spatial coordinate data, these techniques were impractical in our setting.
- **Entropy-based sampling**: Motivated by Zhang, Wang, and X. Li (2016), we explored selecting pixels with high spectral entropy over time, under the assumption that dynamically changing pixels are more informative. Although promising in theory, this method added significant computational cost and showed marginal benefits only in some cases.

Ultimately, we adopted uniform random sampling as our default method due to its simplicity ($O(n)$), speed and consistently competitive performance when compared to more complex alternatives.

Chapter IV

Model Architecture

The crop classification model, denoted as ParcelModel, is designed to classify agricultural parcels into one of eight crop types using the preprocessed *TimeMatch* dataset, specifically the Denmark 2017 subset. By exploiting the spatiotemporal characteristics of Sentinel-2 satellite imagery, the model integrates three meticulously crafted components: the PixelSetEncoder, which extracts spatial features from variable pixel sets; the TransformerTimeEncoder, which models temporal dynamics through attention mechanisms; and the ClassifierHead, which maps learned representations to crop type probabilities. This chapter provides a comprehensive exploration of the theoretical foundations, operational principles and practical suitability of these components for remote sensing tasks, drawing on seminal works to contextualize their design and integration.

The ParcelModel is engineered to process multispectral time series data, capturing both the spatial variability inherent in agricultural parcels and the temporal dynamics across 52 weekly observations. Each parcel comprises a variable number of pixels, each characterized by a sequence of spectral measurements across 12 channels (10 Sentinel-2 bands + NDVI + EVI), accompanied by temporal metadata specifying acquisition dates as day-of-year indices. The model's architecture is tailored to handle this complexity, ensuring robustness against irregular pixel counts and non-uniform temporal sampling. The forward pass, illustrated in Figure I, delineates the sequential processing of input data through the model's components, transforming raw spatiotemporal inputs into class predictions.

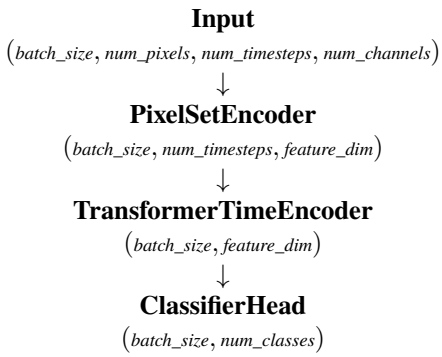

Figure I: Forward pass of the ParcelModel.

I Pixel Set Encoder

Central to the ParcelModel's design is the PixelSetEncoder, which addresses the challenge of processing parcels with variable pixel counts—a common issue in remote sensing due to differences in parcel size and geometry. This component draws inspiration from set-based neural architectures introduced by Zaheer et al. (2017), which model inputs as unordered sets to ensure permutation invariance.

More precisely, the architecture builds upon the work of Garnot et al. (2020), who proposed the Pixel-Set Encoder as an effective mechanism for summarizing spatially distributed pixel-level features into a compact, permutation-invariant representation. This summarization facilitates robust integration of spatial information prior to temporal modeling, which is crucial in high-resolution satellite imagery where intra-parcel heterogeneity can obscure crop-specific patterns. In the context of the *TimeMatch* dataset, the PixelSetEncoder processes each pixel's spectral features—12 channels comprising 10 Sentinel-2 bands augmented with NDVI and EVI—using a shared multi-layer perceptron (MLP). The MLP consists of two linear layers: the first projects the 12-dimensional input to a 64-dimensional hidden space with a ReLU activation, and the second maps this to a 128-dimensional output, producing a feature vector for each pixel at each time step.

To further enhance the encoder's capacity to prioritize informative pixels (e.g., vegetation as opposed to soil or shadows), we integrate a self-attention mechanism inspired by the Transformer architecture of Vaswani et al. (2017). Following the MLP, a linear projection is applied to compute a scalar attention score for each pixel. These scores are normalized via a softmax function across the pixel dimension to yield attention weights, which are used to compute a weighted sum of pixel embeddings.

$$\text{attn\_scores} = W_{\text{attn}} \cdot x, \quad \text{attn\_weights} = \text{softmax}(\text{attn\_scores}),$$
$$x_{\text{agg}} = \sum_{\text{pixels}} (\text{attn\_weights} \cdot x),$$

where x is the MLP output of shape (*batch_size*, 52, *num_pixels*, 128), and W_{attn} is a learned linear transformation producing scalar attention scores. This mechanism enables the model to emphasize pixels containing significant spectral information, thereby generating a more informative and noise-resilient parcel-level representation. The final output of the PixelSetEncoder is a tensor of shape (*batch_size*, 52, 128), representing a temporally ordered sequence of spatially aggregated features, which is subsequently passed to downstream temporal models for classification.

II Transformer Time Encoder

The output of the PixelSetEncoder, which retains temporal and feature dimensions, serves as input to the TransformerTimeEncoder, a component designed to model the temporal evolution of spectral features critical for capturing crop phenology. Phenological patterns, such as the growth stages of winter_wheat or the flowering of spring_barley, are pivotal for distinguishing crop types with overlapping spectral signatures. The TransformerTimeEncoder leverages the Transformer architecture, introduced by Vaswani et al. (2017), renowned for its self-attention mechanism that computes weighted interactions between time steps. This mechanism enables the model to prioritize significant phenological events—such as peak vegetation or senescence—irrespective of their precise timing, a capability particularly suited to the non-uniform temporal patterns in satellite time series, as demonstrated by Rußwurm and Körner (2020). To incorporate temporal context, the encoder employs sinusoidal positional encodings, also proposed by Vaswani et al. (2017), which map day-of-year indices to continuous vectors. These encodings, defined for a time step t and model dimension d_{model} as:

$$\text{PE}(t, 2i) = \sin\left(t/10000^{2i/d_{\text{model}}}\right) \quad \& \quad \text{PE}(t, 2i+1) = \cos\left(t/10000^{2i/d_{\text{model}}}\right),$$

preserve temporal relationships and accommodate variable sequence lengths, ensuring the model captures seasonal cyclicity essential for distinguishing crops like winter_rye from spring_barley.

II.I Attention and CLS Token

The TransformerTimeEncoder incorporates a learnable classification token ([CLS]), inspired by the BERT model developed by Devlin et al. (2018), which aggregates temporal information into a single vector. The [CLS] token is prepended to the sequence, increasing its length. The transformer, configured with 4 attention heads and 2 layers, processes the sequence using multi-head self-attention, allowing the model to focus on critical time steps. The output corresponding to the [CLS] token, of shape (*batch_size*, 128), is extracted as the final parcel representation.

To enhance regularization and prevent overfitting, we added a dropout layer (with a rate of 0.1) after the transformer, following the attention mechanism. Additionally, batch normalization is applied to the [CLS] token output to stabilize training, especially given the small dataset size (4,764 parcels). The final output of the TransformerTimeEncoder is a tensor of shape (*batch_size*, 128), ready for classification.

III Classifier Head

The ClassifierHead constitutes the final stage of the ParcelModel, mapping the aggregated temporal representation to class logits for the eight crop types defined during preprocessing. Implemented as a multi-layer perceptron (MLP), this component exploits the non-linear mapping capabilities of neural networks, as delineated by Hastie, Tibshirani, and Friedman (2009), to delineate complex decision boundaries among crop classes. Dropout regularization mitigates overfitting, a critical issue in remote sensing where labeled data is limited, as established by Belgiu and Drăguţ (2016). The MLP consists of a linear layer mapping the input dimension of 128 to a hidden dimension of 64, followed by batch normalization, a ReLU activation, a dropout layer, and a final linear layer to 8 output classes. The output layer aligns with the filtered label set, excluding underrepresented classes such as spring_peas, ensuring predictions are tailored to the dataset's class distribution.

III.I Loss Function

To quantify our model's performance during training, we employ the Categorical Cross-Entropy loss function, introduced by Goodfellow, Bengio, and Courville (2016). This loss function quantifies the divergence between predicted class probabilities and true labels, making it optimal for multi-class classification tasks. For a given parcel with true class label $y_i \in \{1, \ldots, 8\}$ and predicted probabilities p_i, the loss is computed as:

$$L = -\sum_{i=1}^{8} y_i \log(p_i),$$

where y_i is a one-hot encoded vector representing the true class and p_i is the predicted probability for class i. This formulation penalizes incorrect predictions by assigning higher loss to low-probability assignments for the true class, thereby encouraging the model to assign high confidence to correct crop type predictions, such as distinguishing winter_wheat from spring_barley.

To address class imbalance in the *TimeMatch* dataset (e.g., 1140 spring_barley vs. 275 corn parcels), the loss is weighted using class weights derived from the frequency of each class in filtered_labels.json. The weights are computed as the inverse of the class counts, normalized to sum to the number of classes (8), ensuring that underrepresented classes contribute more to the loss:

$$\text{class\_weights}_i = \frac{1/\text{count}_i}{\sum_{j=1}^{8}(1/\text{count}_j)} \cdot 8,$$

where count_i is the number of samples for class i.

III.II Optimization

Model optimization employs the Adam optimizer, introduced by Kingma and Ba (2014). Adam integrates first-order gradient-based optimization with adaptive moment estimation, computing exponentially weighted moving averages of gradients (first moment) and squared gradients (second moment) to adaptively adjust per-parameter learning rates.For the ParcelModel, this method optimizes the high-dimensional parameter space, encompassing the multi-layer perceptron weights of the ClassifierHead and the attention mechanism parameters of the TransformerTimeEncoder and PixelSetEncoder. The optimizer is configured with a learning rate (α) and a weight decay of 1×10^{-4} for L2 regularization. The algorithm minimizes the weighted Categorical Cross-Entropy loss through iterative updates, defined as:

$$m_t = \beta_1 m_{t-1} + (1-\beta_1) g_t, \quad v_t = \beta_2 v_{t-1} + (1-\beta_2) g_t^2,$$
$$\hat{m}_t = \frac{m_t}{1-\beta_1^t}, \quad \hat{v}_t = \frac{v_t}{1-\beta_2^t}, \quad \theta_{t+1} = \theta_t - \alpha \frac{\hat{m}_t}{\sqrt{\hat{v}_t} + \epsilon},$$

where g_t is the gradient at time t, m_t and v_t are the first and second moment estimates, $\hat{m}_t$ and $\hat{v}_t$ are bias-corrected estimates, α is the learning rate, β_1 and β_2 are exponential decay rates, ϵ is a small constant for numerical stability and θ_t represents model parameters. This formulation ensures efficient convergence for the eight-class classification task. To further enhance convergence, a learning rate scheduler (ReduceLROnPlateau) is employed, which reduces the learning rate by a factor of 0.5 when the validation F1 score plateaus, with a patience of specified epochs.

IV Classification Metrics

The integration of these components within the ParcelModel creates a hierarchical architecture that synergistically exploits spatial and temporal patterns. The PixelSetEncoder reduces spatial complexity by aggregating pixel-level data, the TransformerTimeEncoder captures seasonal dynamics through attention and positional encodings and the ClassifierHead delivers accurate classifications. This design mirrors advanced remote sensing architectures, such as those proposed by Garnot et al. (2020), balancing computational efficiency with expressive power. To evaluate performance, the model employs the ClassificationMetrics class, which computes metrics tailored to multi-class problems. Accuracy and micro-averaged F1-score provide overall performance insights, while weighted F1-score, precision and recall account for class imbalance, such as the disparity between spring_barley (1140 parcels) and corn (275 parcels). The confusion matrix, as emphasized by Congleton and Green (1991), reveals misclassification patterns, facilitating analysis of errors between phenologically similar crops like winter_wheat and winter_barley.

Chapter V

Training

The training process for the ParcelModel optimizes its performance in classifying agricultural parcels into one of eight crop types using the preprocessed *TimeMatch* dataset, specifically the Denmark 2017 subset. This chapter details the training pipeline, implemented in the script train.py, which leverages the spatiotemporal architecture to address challenges such as data variability, class imbalance, and overfitting, ensuring robust and generalizable model performance.

I Dataset Preparation and Splitting

Training begins with the preparation of the *TimeMatch* dataset, utilizing the ParcelDataset class to load and preprocess the multispectral time series data, as outlined in the preprocessing chapter. Our code supports two splitting strategies: a stratified train-test split or K-fold cross-validation, controlled via a command-line argument (–mode).

For the stratified split, the dataset is divided into training (80%) and validation (20%) sets using sklearn.model_selection.train_test_split with stratification based on class labels. This ensures proportional representation of each class in both sets, addressing class imbalance (e.g., 1,140 spring_barley vs. 275 corn parcels).

Alternatively, for K-fold cross-validation, the dataset is split into 5 folds (k_folds=5) with shuffling, as introduced by Kohavi (1995).

The training data is batched with a size of 32 and shuffled to promote stochastic gradient updates, using PyTorch's DataLoader with drop_last=True to ensure consistent batch sizes. The validation data is processed in batches of the same size without shuffling (drop_last=False) to maintain consistency during evaluation.

II Model Initialization and Optimization

The ParcelModel is initialized with its core components: the PixelSetEncoder, TransformerTimeEncoder and ClassifierHead. The encoder maps the 12 input channels (10 Sentinel-2 bands + NDVI + EVI) to a 128-dimensional feature space (in_channels=12, out_dim=128) through a hidden dimension of 64 (hidden_dim=64). The transformer processes the temporal sequence with an input dimension of 128 (input_dim=128), and the classifier outputs logits for the 8 crop classes (num_classes=8). The model is transferred to the available device, preferably a GPU (cuda) or a plain CPU (cpu).

Optimization employs the Adam optimizer, with a learning rate of 10^{-4} (lr=1e-4) and L2 regularization via weight_decay=1e-4. A learning rate scheduler, ReduceLROnPlateau, adjusts the learning rate by a factor of 0.5 if the validation F1-score does not improve for 3 epochs. The loss function is a weighted Categorical Cross-Entropy, to address class imbalance.

III Training & Evaluation Loop

Training proceeds over a maximum of 100 epochs, with each epoch involving a full pass over the training set. In training mode (model.train()), gradients are computed for each batch. The input data: spectral features (x), labels (y) and day-of-year metadata (doy), are moved to the designated device and the optimizer's gradients are zeroed with optimizer.zero_grad(). The model produces class logits through its forward pass and the weighted loss is computed. Gradients are backpropagated with loss.backward() and the optimizer updates the model parameters with optimizer.step(), iteratively minimizing the loss. Progress bars via tqdm monitor batch processing. Following each epoch, the model is evaluated on the validation set in evaluation mode (model.eval()) and gradient computations are disabled with torch.no_grad(). Validation metrics are computed and the scheduler adjusts the learning rate based on the validation weighted F1-score. To prevent overfitting, an early stopping mechanism is employed, as proposed by Prechelt (1998). If the validation weighted F1-score does not improve for 10 consecutive epochs, training halts. The model with the best validation F1-score is checkpointed to disk in the checkpoints/ directory, preserving optimal weights for subsequent evaluation.

IV Final Evaluation and Visualization

After training, we assess the top-performing model using the validation set to gain a clear understanding of its overall effectiveness. This evaluation reveals key performance insights, showcasing how well the model distinguishes between crop types. Notably, the confusion matrix sheds light on classification challenges, especially with phenologically similar crops like winter wheat and winter barley, helping us understand where improvements might be needed.

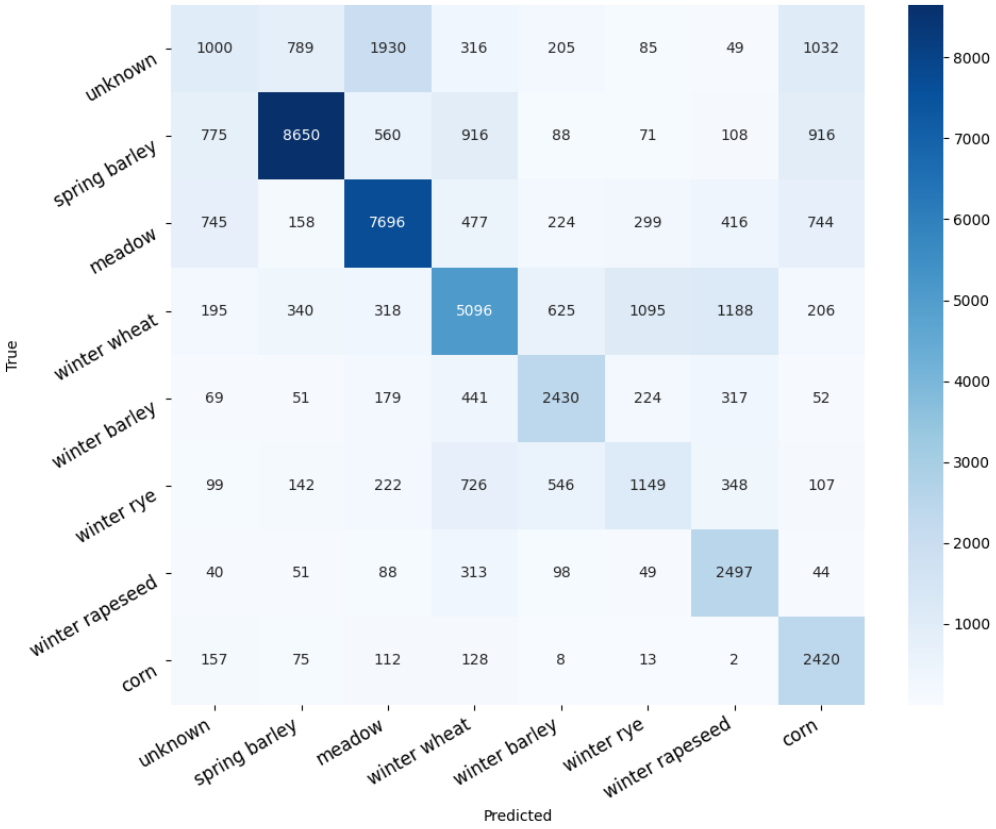

The confusion matrix shows that the model performs well overall, with strong classification accuracy for key classes like meadow, spring_barley and winter_wheat, all having high values along the diagonal. Meadow in particular stands out with over 8600 correct predictions, indicating that it is easily distinguishable. However, there is noticeable confusion between several agriculturally similar classes. For example, spring_barley is often misclassified as winter_wheat and meadow, which is understandable given their likely spectral or seasonal similarities. Winter_wheat also sees frequent misclassification into winter_rye and winter_barley, which are phenologically close and as we saw in Figure I are visually quite similar. Corn is reasonably well predicted, but still shows confusion with other classes, particularly meadow and unknown. The unknown class performs the worst, with significant misclassifications into nearly all other categories, most notably meadow and corn, reflecting its inherently undefined and heterogeneous nature. This broad confusion arises because the unknown class encompasses diverse or ambiguous samples that do not clearly belong to any specific class, making it inherently difficult for the model to learn. Overall, while core crop types are recognized well, the model struggles with edge cases and visually similar cereals, highlighting the need for improved feature discrimination or enhanced training data representation.

To capture the model's learning trajectory, we present training curves that track the training loss and validation F1-score over time. These plots provide a clear, high-level view of how the model's performance evolves during training, highlighting both its learning progress and generalization ability.

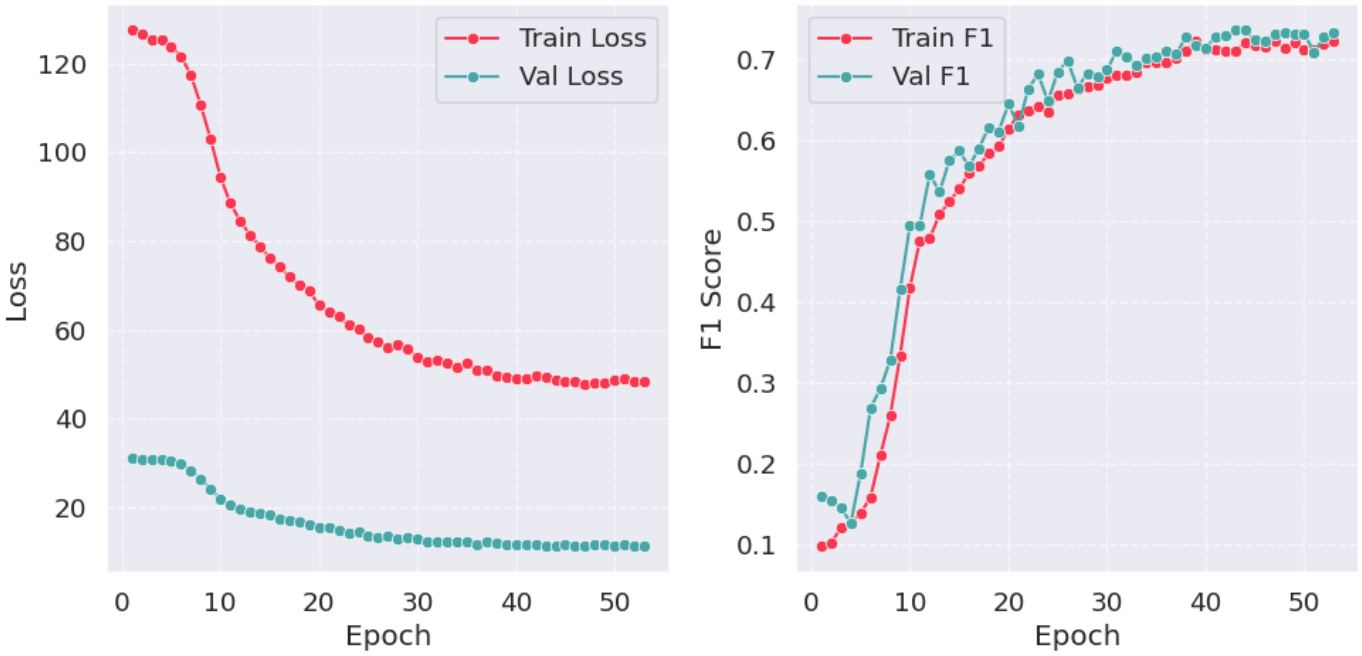

Figure I: Training Metrics

In the figure above, the training loss consistently decreases but remains higher than the validation loss. This behavior is attributed to the training phase, where parcels are sampled rather than using their full pixel representation, combined with the application of extensive data augmentation. The training F1 score exhibits a steady improvement, while the validation F1 score, although slightly more variable, follows a similar upward trend. Ultimately, the validation F1 score plateaus, and the learning process is terminated by the early stopping mechanism.

Bibliography

[1] Mariana Belgiu and Lucian Drăguţ. “Random Forest in Remote Sensing: A Review of Applications and Future Directions”. In: *ISPRS Journal of Photogrammetry and Remote Sensing* 114 (2016), pp. 24–31.

[2] Russell G. Congleton and Robert O. Green. “A Review of Remote Sensing Accuracy and Error Assessment”. In: *Photogrammetric Engineering and Remote Sensing* 57.11 (1991), pp. 1441–1447.

[3] Jacob Devlin et al. *BERT: Pre-training of Deep Bidirectional Transformers for Language Understanding*. arXiv preprint arXiv:1810.04805. 2018.

[4] Yuval Eldar et al. “Farthest point strategy for progressive image sampling”. In: *IEEE Transactions on Image Processing* 6.9 (1997), pp. 1305–1315.

[5] Vivien S. F. Garnot et al. “Satellite Image Time Series Classification with Pixel-Set Encoders and Temporal Self-Attention”. In: *Conference on Computer Vision and Pattern Recognition (CVPR)*. 2020.

[6] Ian Goodfellow, Yoshua Bengio, and Aaron Courville. *Deep Learning*. MIT Press, 2016.

[7] Trevor Hastie, Robert Tibshirani, and Jerome Friedman. *The Elements of Statistical Learning: Data Mining, Inference, and Prediction*. 2nd ed. Springer, 2009.

[8] Alfredo Huete et al. “Overview of the radiometric and biophysical performance of the MODIS vegetation indices”. In: *Remote Sensing of Environment* 83.1-2 (2002), pp. 195–213.

[9] Diederik P Kingma and Jimmy Ba. “Adam: A Method for Stochastic Optimization”. In: *arXiv preprint arXiv:1412.6980* (2014).

[10] Ron Kohavi. “A Study of Cross-Validation and Bootstrap for Accuracy Estimation and Model Selection”. In: *Proceedings of the International Joint Conference on Artificial Intelligence (IJCAI)* 14.2 (1995), pp. 1137–1145.

[11] Jie Li and Andrew D Heap. “Spatial sampling design for monitoring spatial phenomena”. In: *Geographical Analysis* 47.3 (2015), pp. 207–228.

[12] J. MacQueen. “Some methods for classification and analysis of multivariate observations”. In: *Proceedings of the fifth Berkeley symposium on mathematical statistics and probability*. Vol. 1. 14. 1967, pp. 281–297.

[13] Lutz Prechelt. “Early Stopping – But When?” In: *Neural Networks: Tricks of the Trade* (1998), pp. 55–69.

[14] Marc Rußwurm and Marco Körner. “Self-Attention for Raw Optical Satellite Time Series Classification”. In: *ISPRS Journal of Photogrammetry and Remote Sensing* 169 (2020), pp. 421–435.

[15] Steven K Thompson. *Sampling*. John Wiley & Sons, 2012.

[16] Ashish Vaswani et al. “Attention is All You Need”. In: *Advances in Neural Information Processing Systems (NeurIPS)*. 2017.

[17] Manzil Zaheer et al. “Deep Sets”. In: *Advances in Neural Information Processing Systems (NeurIPS)* (2017).

[18] Li Zhang, Yi Wang, and Xi Li. “An entropy-based sampling method for remote sensing image classification”. In: *IEEE Geoscience and Remote Sensing Letters* 13.5 (2016), pp. 631–635.